JOURNAL OF APPLIED ELECTROCHEMISTRY 17 (1987) 185–195

The impedance of alkaline manganese cells and their relationship to cell performance. III. Correlation with high-rate pulse discharge capacity

R. BARNARD, L. M. BAUGH*, C. F. RANDELL

Ever Ready Limited, Technical Division, Tanfield Lea, Stanley, Co. Durham, UK

Received 26 March 1986; revised 25 April 1986

The extent to which the initial impedance characteristics of a batch of LR6 alkaline manganese cells determine their life and therefore capacity during a typical 2 A/10 s pulse discharge regime has been investigated, and the importance of thermodynamic factors have also been considered. It is shown that the potential drop ($E - V_{pulse}$) for the initial discharge cycle can be calculated approximately from a knowledge of the initial internal resistance value, and the recovery voltage, V_{rec}, can be calculated using a simple thermodynamic theory for the homogeneous phase discharge of γ-MnO_2. During subsequent cycles the polarization of the cathode–can assembly remains approximately constant at 300 mV while that of the anode–separator system increases progressively from 100 mV to > 300 mV. The constancy of the former parameter can be attributed to constancy in the cathode contribution to the internal resistance, whereas the changes in the latter can be ascribed to increases in anode resistance polarization and anode concentration polarization. Minimization of cell internal resistance and anode polarization are therefore of primary concern if cell performance is to be maximized.

Nomenclature

E	initial open-circuit voltage
V_{pulse}	cell voltage at $t = 10$ s
$\bar{V}_{pulse}$	cell voltage at $t = 10$ s for the first pulse
V_{rec}	open-circuit voltage at the end of a 50-s recovery period
ΔV	total polarization of the cell
ΔV_A	anode polarization (anode–separator system)
ΔV_C	cathode polarization (cathode–can assembly)
η_Ω	ohmic polarization
η_{CT}	charge-transfer polarization
η_C	concentration polarization
R_i	cell internal resistance
R_e	electrolyte resistance
R_{part}^{cath}	contact resistance between cathode particles or within the particles themselves
R^{cath}	effective resistance of cathode–can assembly
R_1^{cath}	contact resistance at the interface between the nickel oxide phase and the cathode (MnO_2 + graphite mixture)
R_{phase}^{cath}	resistance of the nickel oxide phase on the surface of the nickel-plated steel positive current collector (cell can)
R_2^{cath}	contact resistance at the interface between the nickel oxide layer on the can surface and the can itself
R'	high frequency intercept on complex plane impedance diagram
R''	diameter of the complex plane impedance semicircle
f^*	characteristic frequency at the top of the complex plane semicircle
C	effective parallel capacitance in the equivalent circuit for a cell attributed to the cathode–can assembly
c_{MnO_2}	concentration of MnO_2 at any point in the discharge

* *Present address*: BNF Metals Technology Centre, Grove Laboratories, Denchworth Road, Wantage, Oxon, UK.

0021–891X/87 $03.00 + .12

$c^0_{MnO_2}$ maximum MnO_2 concentration at 100% efficiency
c_{MnOOH} concentration of MnOOH at any point in the discharge
c^0_{MnOOH} maximum MnOOH concentration at 100% efficiency
ψ proton–electron spatial correlation coefficient
I total current
$i_{R''}$ current through resistance R''
i_c current through capacitor
V_p voltage drop across parallel R–C circuit

Superscripts
A anode
C cathode
obs observed
calc calculated

1. Introduction

In the previous paper [1] the theory relating the short-circuit current to the internal resistance of primary cells was reviewed and tested in the case of both alkaline manganese and Leclanché cells. The initial 2-A pulse discharge behaviour of alkaline manganese cells was also examined and correlated satisfactorily with the internal resistance value. Earlier it had been demonstrated that the internal resistance is a composite of many variables, several of which can be resolved independently using *in situ* impedance techniques [2]. The present communication is concerned with an investigation to determine the extent to which the initial impedance characteristics of a cell determines its life and hence capacity during a typical high-rate pulse discharge regime. The regime chosen was 2 A for 10 s followed by a 50 s recovery period.

2. Experimental details

The experimental methods used in the present work have been described previously [1, 2]. Two groups of LR6 cells were examined and these are designated Group 1 and Group 2. However, most of the reported results are for Group 1 cells.

3. Results and discussion

3.1. *Factors which determine the general shape of the discharge curve and calculation of the thermodynamic variable* V_{rec}

Fig. 1a shows a typical first discharge cycle. The pulse profile is very similar to that discussed earlier in connection with LR20 cells [1]. During the on-load period the pulse profile consists of an instantaneous voltage drop followed by a shoulder culminating in an almost constant voltage at 10 s. During the off-load period there is an equivalent instantaneous voltage drop followed by a voltage recovery. Fig. 1b shows the on-load and off-load voltages as a function of cycle number during a typical discharge regime. In Fig. 1, E is the initial cell voltage of 1.56 V, V_{pulse} is the on-load cell voltage at the end of the 10 s discharge period and V_{rec} is the off-load cell voltage at the end of the 50 s recovery period. A cell is deemed to 'fail' on a typical pulse discharge regime when $V_{pulse} < 0.6$ V, i.e. when the voltage loss,

$$(E - V_{pulse}) > 0.96\,V \quad (1)$$

In Fig. 1b the quantity $(V_{rec} - V_{pulse})$ is equal to the total polarization of the electrode systems anode + separator and cathode + can

$$(V_{rec} - V_{pulse}) = (\Delta V_A + \Delta V_c) \quad (2)$$

where ΔV_A is the potential drop across the anode–separator system and ΔV_c is the potential drop across the cathode–can assembly. From Fig. 1b and Equations 1 and 2 it is clear that a cell fails when

$$(E - V_{rec}) + (\Delta V_A + \Delta V_c) > 0.96\,V \quad (3)$$

It can be seen from Equation 3 that the rate at which a cell fails increases with decrease in V_{rec} and increase in ΔV_A and ΔV_c. It is therefore essential to understand the factors which determine the magnitude of these parameters. In the case of V_{rec} only thermodynamic principles pertain because no net current flow is involved and the electrode reactions can therefore be assumed to be in a state of pseudo-equilibrium. However, in the case of ΔV_A and ΔV_c it is necessary to consider kinetic factors since the total polarization at either electrode system consists of

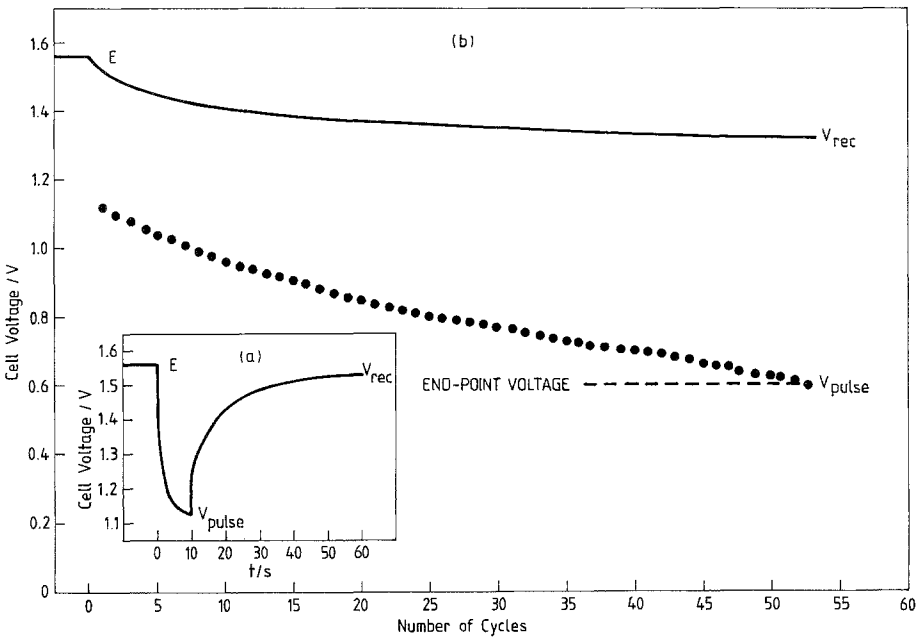

Fig. 1. (a) Typical initial pulse profile for an LR6 cell indicating the important variables E, V_{pulse} and V_{rec}; (b) typical discharge curve indicating values of V_{pulse} and V_{rec} as a function of cycle number.

several components:

$$\Delta V = \eta_\Omega + \eta_{ct} + \eta_c \qquad (4)$$

The calculation of V_{rec} from first principles provides further insight into the variables which control the overall shape of the discharge curve. Experiments conducted with the specially constructed zinc reference electrodes, described previously [2], showed that the variation in V_{rec} can be attributed exclusively to the manganese dioxide electrode, since the potential of the zinc electrode was always found to recover completely after each discharge cycle. The manganese dioxide reaction can be represented

$$MnO_2 + e + H_2O \rightleftharpoons MnOOH + OH^- \qquad (5)$$

This is a homogeneous reaction involving the injection of protons and electrons into the MnO_2 lattice. During discharge the concentration of MnO_2 within the lattice decreases continuously whilst that of MnOOH increases continuously. The activities of MnO_2 and MnOOH at any point in the discharge are given by

$$a_{MnO_2} = c_{MnO_2}/c^0_{MnO_2} \qquad (6)$$

and

$$a_{MnOOH} = c_{MnOOH}/c^0_{MnOOH} \qquad (7)$$

Furthermore,

$$a_{MnO_2} + a_{MnOOH} = 1 \qquad (8)$$

The thermodynamic potential of the MnO_2–MnOOH mixture is found to obey a modified Nernst equation [3],

$$V^{calc}_{rec} = E_0 + (\psi RT/nF) \ln (a_{MnO_2}/a_{MnOOH}) \qquad (9)$$

where ψ is the proton–electron spatial correlation coefficient [4, 5]. In γ-MnO_2, ψ has a value of 2 [3]. If E^0 is the standard potential of the MnO_2–MnOOH electrode on a potential scale referred to that of zinc in the same working electrolyte, then E^0 can be determined from the initial cell voltage (1.56 V):

$$E^0 = 1.56 - (2RT/nF) \ln (a'_{MnO_2}/a'_{MnOOH}) \qquad (10)$$

It can be seen from Equations 9 and 10 that in order to calculate V_{rec} as a function of time, a value for the initial activity ratio a'_{MnO_2}/a'_{MnOOH} must be known and also some assumption must be made as to how a_{MnO_2}/a_{MnOOH} changes with

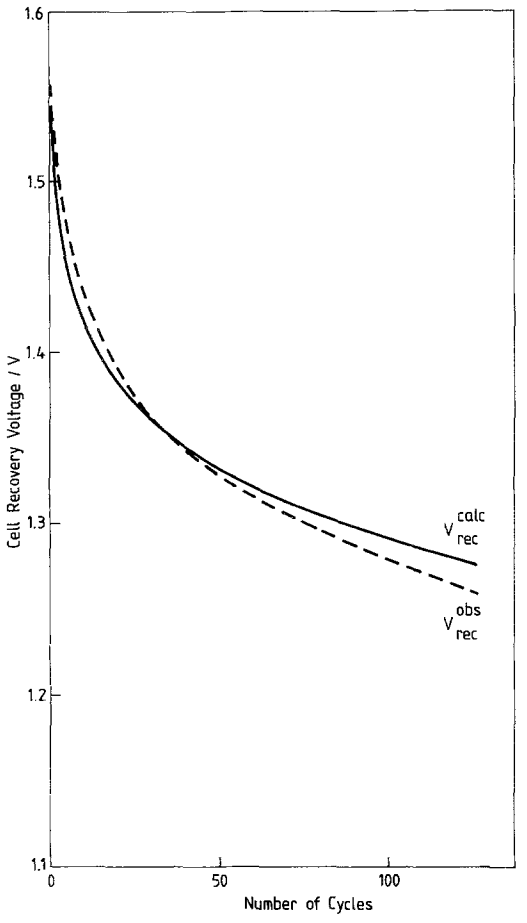

Fig. 2. Relationship between observed and calculated V_{rec} values and cycle number for LR6 cells.

cycle number. Using an iterative procedure it was found that the best fit of observed and calculated V_{rec} data could be obtained when $a'_{MnO_2} = 0.9986$ and $a'_{MnOOH} = 0.0014$ assuming also that a_{MnO_2} decreases and a_{MnOOH} increases by a factor of 20/9100 = 0.0022 during each discharge cycle, i.e. 20 coulombs are extracted per cycle from a theoretical capacity of 9100 coulombs. This leads to $E^0 = 1.22$ V. Fig. 2 shows a plot of V_{rec}^{calc} and V_{rec}^{obs} versus cycle number up to 120 cycles. The agreement between these parameters is very good considering the simple theoretical analysis used to determine V_{rec}^{calc} and the fact that V_{rec}^{obs} may not be absolutely at equilibrium.

The attainment of a theoretical basis for V_{rec} in Fig. 1b is clearly important because it establishes the sloping base line from which the value of V_{pulse} is ultimately determined. However, it can be seen from Fig. 1b that irrespective of cycle number, the potential loss $(E - V_{rec})$ represents only about 25% of the total loss $(E - V_{pulse})$ in the case of the Group 1 cells illustrated. This simple observation serves to demonstrate further the well-known fact that equilibrium thermodynamic considerations are of secondary importance in determining high-rate cell performance.

3.2. *Calculation of the potential drop* $(E - V_{pulse})$ *for the initial discharge cycle from the initial impedance spectrum and comparison with experiment*

In order to calculate values for V_{pulse} it is necessary to establish the extent to which the parameters in Equation 4 participate within the 10 s time scale that the cell is discharged, since for the first cycle

$$(E - V_{pulse}) = (\Delta V_A + \Delta V_c) = (\eta_\Omega^A + \eta_\Omega^C) + (\eta_{CT}^A + \eta_{CT}^C) + (\eta_C^A + \eta_C^C) \quad (11)$$

where the subscripts and superscripts A and C refer to the anode–separator system and cathode–can assembly, respectively. In earlier work [1] it was shown that within the time scale of a 4-s pulse the potential response of LR20 cells is controlled predominantly by their internal resistance. Thus $\eta_\Omega \gg \eta_{CT}$ or η_C. The internal resistance value which determines η_Ω was deemed to be composed predominantly of six components, several of which were separated

$$R_i = R_e^{an} + R_e^{cath} + R_{part}^{cath} + R_1^{cath} + R_{phase}^{cath} + R_2^{cath} \quad (12)$$

Equation 12 can be simplified to

$$R_i = R_e + R^{cath} \quad (13)$$

Fig. 3a shows a typical impedance spectrum for a cell in Group 1 obtained at high to medium frequencies. This spectrum is very similar to that obtained previously for LR20 cells from which pulse discharge behaviour can be predicted [1]. The equivalent circuit is shown in Fig. 3b where the semicircle represents an envelope drawn over two smaller semicircles characteristic of indi-

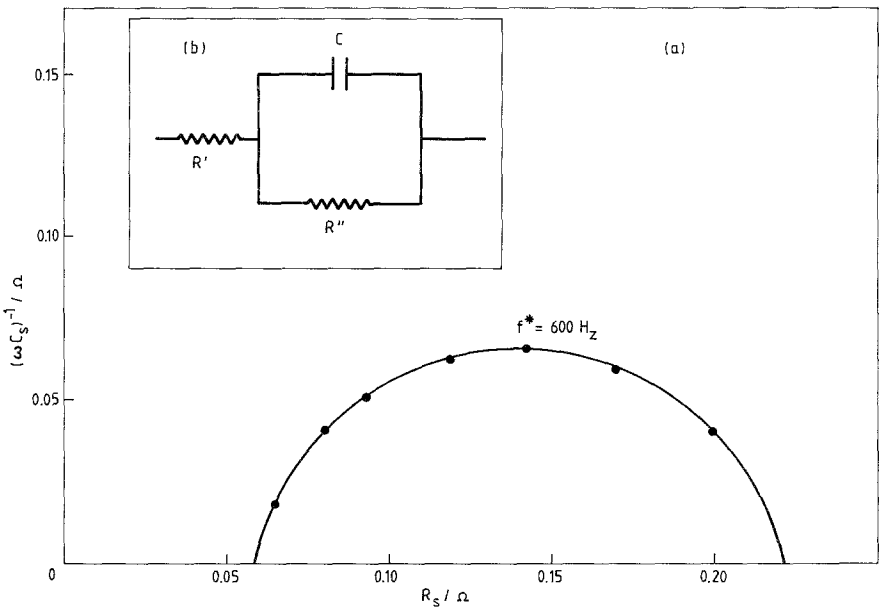

Fig. 3. (a) Typical high frequency impedance spectrum for an LR6 alkaline manganese cell; (b) equivalent circuit.

vidual cathode and can impedances, the relative sizes of which varies according to the exact cell formulation [2]. From this circuit the relationship between potential and time can be determined theoretically and the derivation of the relevant equation is given in the Appendix. This is

$$V = E - I\{R' + R'' - R'' \exp[-t/(RC)]\} \quad (14)$$

From Equation 14 two limiting cases can be defined. Firstly, when $t \to 0$, then $\exp(-t/R''C) \to 1$, and Equation 14 reduces to

$$V = E - IR' \quad (15)$$

where IR' is the instantaneous potential drop on-load or off-load. Secondly, when $t \to \infty$, $\exp(-t/R''C) \to 0$, and Equation 14 becomes

$$V = E - I(R' + R'') = E - IR_i \quad (16)$$

where V is the almost constant voltage plateau after the shoulder in Fig. 1a.

Table 1 summarizes experimental values of R', R'', f^* and C for eight cells in Group 1, and Fig. 4 shows the calculated potential–time profiles over the whole performance range including the profile for an 'average' cell. It is clear from this figure that the potential plateau is achieved very early in the course of the pulse and lies in the range 1 to 10 ms. This time scale agrees well with that determined experimentally in the case of LR20 cells [1]. Table 1 also compares V_{pulse} values calculated from Equation 16 with

Table 1. Initial impedance parameters, calculated and observed V_{pulse} values and cycle lives for cells in Group I

Cell	*R' (Ω)*	*R'' (Ω)*	*(R' + R'') (Ω)*	*f* (Hz)*	*C (F)*	V_{pulse}^{calc} *(V)*	V_{pulse}^{obs} *(V)*	*No. of cycles*
1	0.06	0.16	0.22	600	0.0017	1.12	1.12	53
2	0.06	0.21	0.27	310	0.0024	1.02	1.07	46
3	0.06	0.17	0.23	440	0.0021	1.10	1.07	43
4	0.09	0.26	0.35	310	0.0020	0.86	0.88	29
5	0.10	0.28	0.38	310	0.0018	0.80	0.86	23
6	0.11	0.31	0.42	310	0.0017	0.72	0.79	22
7	0.13	0.27	0.40	310	0.0019	0.76	0.72	22
8	0.22	0.40	0.62	210	0.0019	0.32	0.43	0

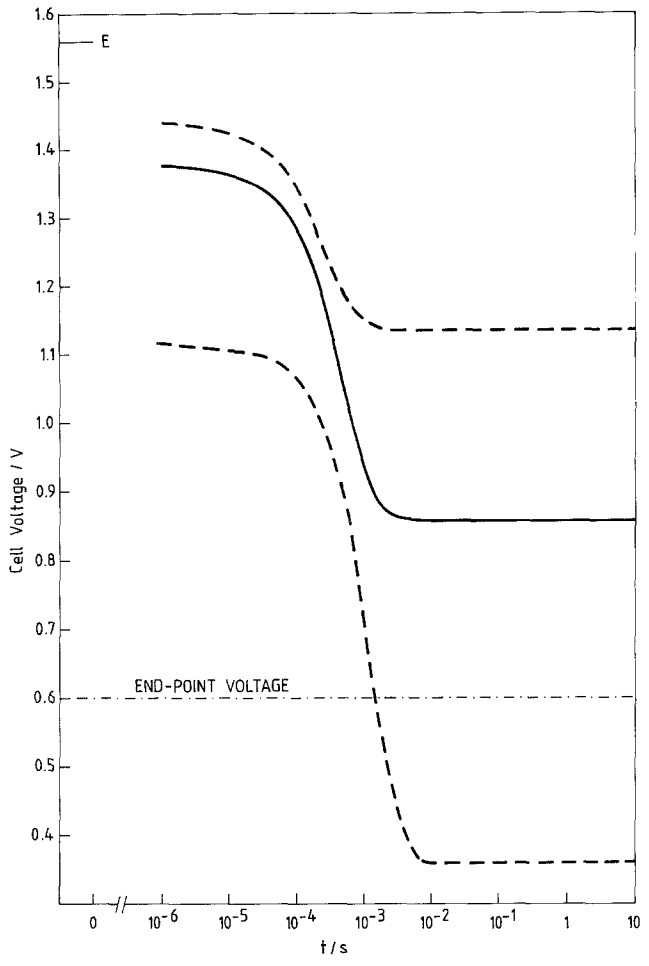

Fig. 4. Plot of calculated cell voltage versus time during the early stages of a 2 A pulse discharge. (——) Typical profile; (- - - -) profiles for cells with lowest and highest internal resistance values.

those determined experimentally. Good agreement between these two parameters is obtained and this is further demonstrated in Fig. 5 which shows V_{pulse}^{calc} and V_{pulse}^{obs} plotted against each other. Except for the cell showing the smallest V_{pulse} value, all other points lie close to the line of unit slope with only small scatter. This is an important result because it demonstrates that a knowledge of the impedance spectrum for a cell allows V_{pulse} for the initial discharge cycle to be calculated. This in turn has a direct bearing on the number of discharge cycles which can be extracted from the cell before the end-point voltage is achieved. The maximum cycle number is also given in Table 1. Nevertheless, the correlation between V_{pulse}^{calc} and V_{pulse}^{obs} which is proven in the case of the Group 1 cells when the equivalent circuit shown in Fig. 4 is used, may not always be observed, since it depends on the MnO_2 polarization at the 10 s time interval being small compared with the total ohmic polarization of the cell, i.e. $\eta_C^C \ll \eta_\Omega$ in Equation 11. For cells with extremely low internal resistance values this approximation is no longer valid since $\eta_C^C \rightarrow \eta_\Omega$.

3.3. *Variation of* $(V_{rec} - V_{pulse})$ *with cycle number and comparison of observed and calculated* ΔV_A *and* ΔV_C *values*

Having established the voltage–time response for the initial discharge pulse on a theoretical basis and linked this quantitatively with the initial impedance spectrum, further work was undertaken in order to assess how $(V_{rec} - V_{pulse})$

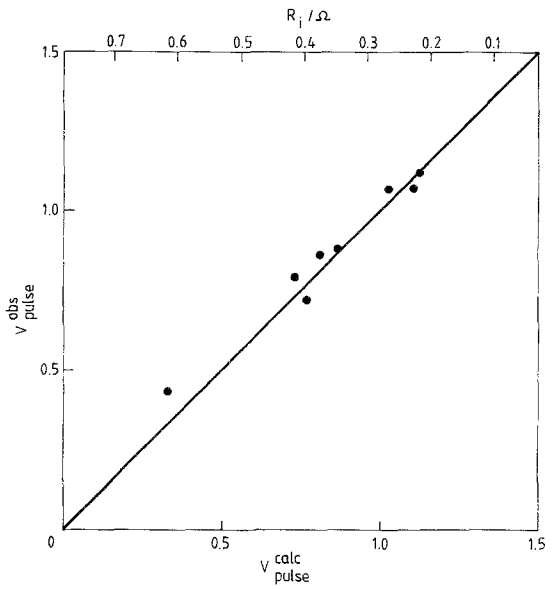

Fig. 5. Correlation between the initial pulse voltage of LR6 cells calculated from their internal resistance values (indicated on upper scale) and the observed initial pulse voltage. Line is drawn with unit slope.

changes with cycle number, since the greater this change the smaller the cell life and hence capacity. Obviously, a knowledge of the changes in the overall impedance spectrum with time on-load would be an equivalent approach to potential measurements because this would permit $(V_{rec} - V_{pulse})$ to be calculated in the manner described above. More specifically, the contribution to changes in the overall impedance spectrum from the anode–separator system and cathode–can assembly would need to be ascertained separately if any detailed understanding of the factors contributing to failure were required. This was, however, beyond the scope of the present investigation. Nevertheless, direct potential measurements on the individual anode and cathode systems were made as a function of cycle number using the reference electrode technique described previously [2]. Fig. 6 shows plots of ΔV_A and ΔV_C as a function of cycle number up to the point of failure. It can be seen that ΔV_C remains approximately constant at ~ 300 mV whereas ΔV_A increases progressively from ~ 100 mV to 400 mV. Thus at the start of discharge the major contributor to the voltage loss is the cathode, whereas towards the end of discharge it is the anode. It may be supposed that the approximately constant cathode polarization arises as a result of constancy in the cathode contribution to the internal resistance value, which from Equation 12 is

$$R_i^{cath} = R_e^{cath} + R_{part}^{cath} + R_1^{cath} + R_{phase}^{cath} + R_2^{cath} \quad (17)$$

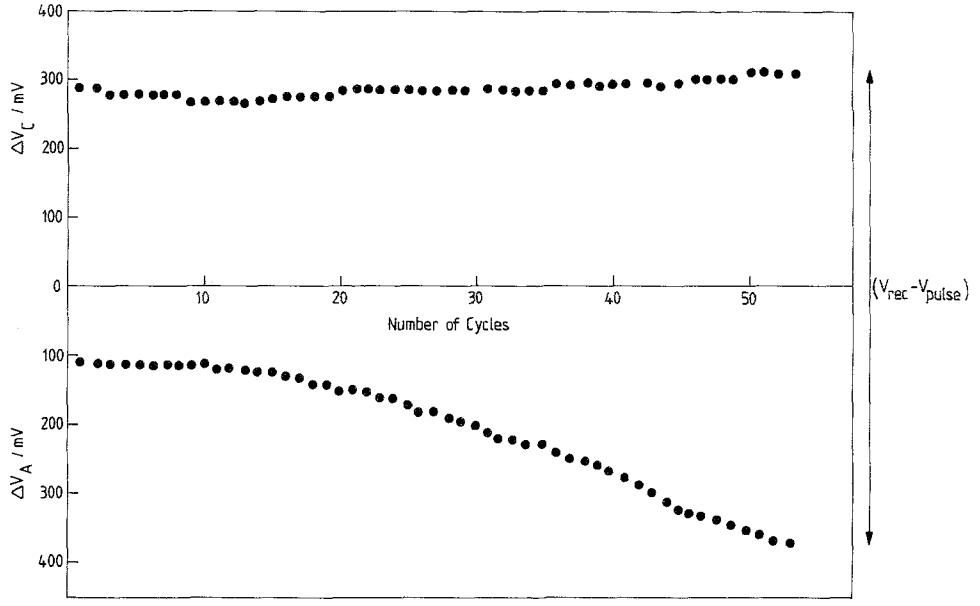

Fig. 6. Polarization of the cathode–can assembly and anode–separator system for a typical LR6 cell as a function of cycle number.

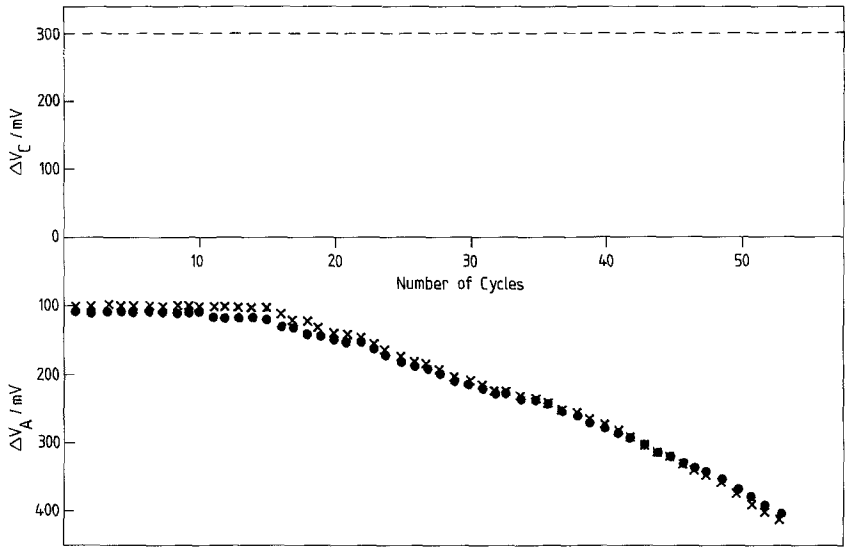

Fig. 7. Comparison of anode polarization curves for a typical LR6 cell: (●) observed; (×) calculated assuming constancy of cathode–can polarization as indicated by dotted line.

The factors which contribute to changes in ΔV_A are probably also numerous. It seems likely that an increase in concentration polarization resulting from the increasing tortuosity and a decrease in volume fraction within the anode due to ZnO formation are probably important, together with increasing ohmic polarization due to the decreasing electrolyte conductivity.

The use of reference electrodes to determine individual changes in the anode and cathode polarizations as a function of cycle number is a time consuming process, particularly for a large batch of cells. However, the polarization characteristics depicted in Fig. 6 can be derived from the V_{pulse}^{obs} value for the initial pulse together with V_{pulse}^{obs} values for subsequent pulses. Central to this calculation is the fact that ΔV_A for the first pulse is invariant at approximately 0.1 V but changes progressively with cycle number. Conversely, ΔV_C is variable for the first cycle but remains approximately constant at 0.3 V throughout the discharge. Thus for any cell

$$\Delta V_C \approx (E - \bar{V}_{pulse}^{obs}) - 0.1 \qquad (18)$$

for the first cycle and subsequent cycles where $\bar{V}_{pulse}^{obs}$ refers to the initial pulse only. Also,

$$\Delta V_A = (V_{rec} - V_{pulse}^{obs}) - \Delta V_C \qquad (19)$$

so that a combination of Equations 18 and 19 leads to

$$\Delta V_A^{calc} = (V_{rec} - V_{pulse}^{obs}) - (E - \bar{V}_{pulse}^{obs}) + 0.1 \qquad (20)$$

It can be seen from Equation 20 that all the quantities on the right hand side are known and hence ΔV_A can be determined as a function of cycle number. Fig. 7 compares calculated and observed values of ΔV_A. It is clear that an excellent agreement is obtained, fully vindicating the simple analysis.

3.4. *Relationship of initial impedance to cell life and capacity*

It is obvious from Fig. 1b that the larger the value of $(E - V_{pulse})$ for the initial discharge cycle the shorter the cell life and hence the lower the cell capacity. This is confirmed in Table 1. Moreover, since $(E - V_{pulse})$ can be correlated directly with the initial impedance spectrum then a relationship would also be expected between the initial impedance and cell capacity. If the anode and cathode polarizations remained constant throughout the discharge then a linear relationship between the initial impedance parameter R_i or $(E - V_{pulse})$ and cycle number would be expected. This situation does not occur because ΔV_A increases as discussed above.

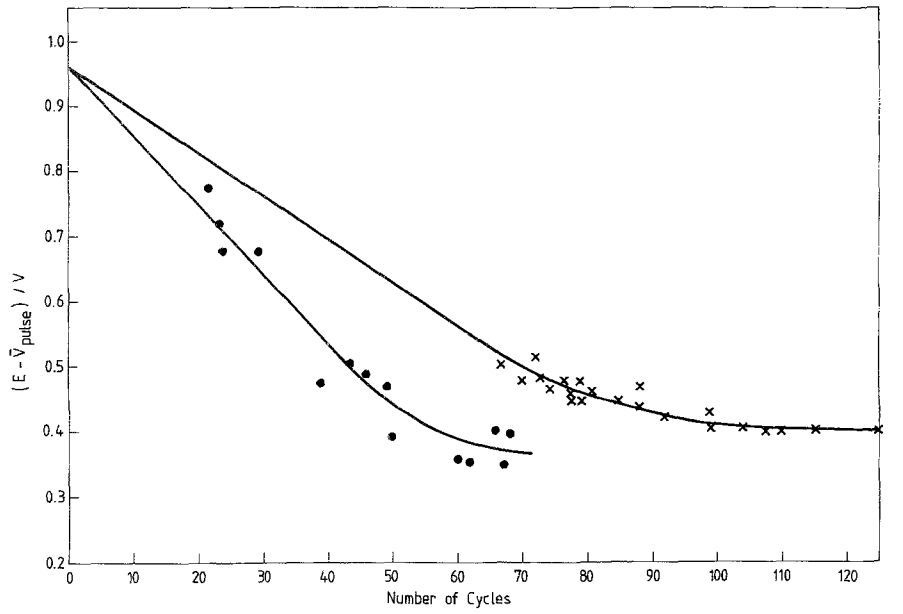

Fig. 8. Potential drop during the first discharge cycle as a function of the total number of available cycles for two groups of LR6 cells: (●) group 1; (×) group 2.

Nevertheless, for small cycle numbers in the range 1 to 20 cycles, Fig. 6 indicates that ΔV_A is very nearly constant. It might then be assumed that a plot of $E - V_{pulse}$ or R_i versus cycle number would be linear in the range of low cycle numbers. Fig. 8 provides some support for this hypothesis where the data for a second batch of cells, Group 2, is also shown. At high cycle numbers where ΔV_A begins to change, curvature is obtained as expected. It can also be seen from Fig. 8 that the Group 2 cells, which have lower internal resistances, perform much better and provide maximum lives of 125 cycles. Interestingly, the curves for the two batches of cells are of a similar shape but they are not superimposable, and this can be explained if it is assumed that ΔV_A increases more rapidly with cycle number for cells in Group 1 than Group 2.

The above results clearly demonstrate the importance of the initial impedance spectrum in determining cell capacity on a high-rate pulse discharge regime. However, they also indicate the need to observe changes in the impedance spectrum as a function of cycle number if a proper understanding of all the factors determining cell life are to be obtained. In particular, the factors determining changes in the impedance of the anode, both on-load and off-load, require systematic investigation. An approach to this problem using a galvanostatic pulse technique has recently been made by Cheeseman and Stock [6].

4. Conclusions

1. Ohmic polarization resulting from significant internal resistance is the important factor which predominantly determines the capacity of the LR6 alkaline manganese cells tested on the 2 A/10 s pulse discharge regime.

2. The potential drop $(E - V_{pulse})$ for the initial discharge cycle can be calculated from a knowledge of the initial impedance spectrum for the cell.

3. The recovery voltage, V_{rec}, can be calculated using a simple thermodynamic theory for the homogeneous phase MnO_2 discharge reaction.

4. During subsequent discharge cycles the polarization of the cathode–can assembly remains approximately constant at 300 mV, while that of the anode–separator system increases progressively from 100 mV to > 300 mV. The constancy of the former parameter can be attributed to constancy in the

cathode contribution to the internal cell resistance, whereas changes in the latter can be ascribed to increases in anode resistance polarization and anode concentration polarizations.

5. The anode and cathode polarizations can be calculated as a function of cycle number from a knowledge of the initial impedance spectrum for the cathode–can assembly and changes in V_{pulse} and V_{rec} only.

6. Minimization of cell internal resistance and anode polarization are required to maximize cell performance during high-rate pulse discharges.

Acknowledgement

The authors wish to thank the Directors of British Ever Ready Limited for permission to publish this work.

Appendix

Relationship between cell voltage and time during the early stages of a galvanostatic discharge

Using the equivalent circuit shown in Fig. A1, the relationship between cell voltage and time can be derived as follows. Kirchoff's laws state that the algebraic sum of the e.m.f.s within the circuit shown must be zero. Hence

$$E = V + IR' + V_p \quad \text{(A1)}$$

Also,

$$I = i_{R''} + i_c \quad \text{(A2)}$$

But

$$i_{R''} = V_p/R'' \quad \text{(A3)}$$

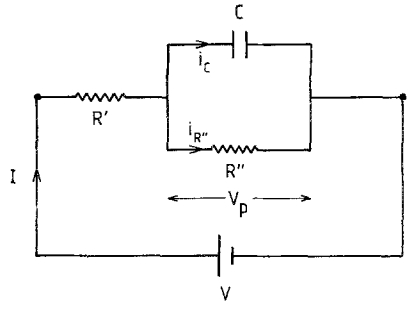

Fig. A1. Equivalent circuit for a discharging LR6 cell showing the on-load potential, V, and the potential drop, V_p, across the parallel R–C together with the respective current values I, $i_{R''}$ and i_c.

and

$$i_c = C(dV/dt) \quad \text{(A4)}$$

$\therefore$ Substituting Equations A3 and A4 into A2

$$I = V_p/R'' + C(dV/dt) \quad \text{(A5)}$$

Rearranging Equation A5

$$dV/dt = -V_p/R''C + I/C \quad \text{(A6)}$$

This is a differential equation of the form

$$dx/dt = ax + b \quad \text{(A7)}$$

where $a = -I/R''C$, $x = V_p$ and $b = I/C$.

The general solution to Equation A7 is

$$t = \int 1/(ax + b) \quad \text{(A8)}$$

which is a standard integral where

$$t = (1/a) \ln Z(ax + b) \quad \text{(A9)}$$

where Z is the integration constant.

Substitution of a, b and x into Equation A9 gives

$$t = -R''C \ln Z[-V_p/(R''C) + I/C] \quad \text{(A10)}$$

The exponential form of Equation A10 is

$$\exp[-t/(R''C)] = Z[(-V_p + IR'')/(R''C)] \quad \text{(A11)}$$

In order to calculate Z, the boundary condition at $t = 0$ must be inserted into Equation A11. At $t = 0$ the voltage across the parallel resistor and capacitor is zero so that $V = E - IR'$ and $V_p = 0$. Substitution into Equation A11 yields

$$1 = Z[(IR'')/(R''C)] \quad \text{(A12)}$$

$$\therefore Z = (R''C)/(IR'') \quad \text{(A13)}$$

Substituting Equation A13 into All yields

$$\exp[-t/(R''C)] = (R''C)/(IR'')\,[(-V_p + IR'')/(R''C)] \quad \text{(A14)}$$

$$= (-V_p + IR'')/(IR'') \quad \text{(A15)}$$

Hence

$$V_p = IR''\{1 - \exp[-t/(RC)]\} \quad \text{(A16)}$$

and substituting Equation A16 into A1

$$E = V + IR' + IR''\{1 - \exp[-t/(RC)]\} \quad \text{(A17)}$$

$$\therefore V = E - IR' - IR''\{1 - \exp[-t/(RC)]\} \quad \text{(A18)}$$

or

$$V = E - I\{R' + R'' - R'' \exp[-t/(RC)]\}$$

which is Equation 14.

References

[1] R. Barnard, L. M. Baugh and C. F. Randell, *J. Appl. Electrochem.* **17** (1987) 174.

[2] *Idem, ibid.* **17** (1987) 165.

[3] R. S. Crandall, F. J. Wolfowicz and B. W. Faugnan, *Solid State Commun.* **18** (1976) 1409.

[4] R. Barnard, C. F. Randell and F. L. Tye, *J. Appl. Electrochem.* **10** (1980) 127.

[5] *Idem, J. Electroanal. Chem.* **119** (1981) 17.

[6] P. G. Cheeseman and M. G. Stock, in 'Power Sources 10' (edited by L. J. Pearce), Paul Press, London (1985) p. 217.